Reducing Drift in Differential Tracking

Ali Rahimi, Louis-Philippe Morency, and Trevor Darrell

Massachusetts Institute of Technology

Computer Science and AI Lab

Cambridge, MA 02139, USA

Abstract

We present methods for turning pair-wise registration algorithms into drift-free trackers. Such registration algorithms are abundant, but the simplest techniques for building trackers on top of them exhibit either limited tracking range or drift. Our algorithms maintain the poses associated with a number of key frames, building a view-based appearance model that is used and refined during tracking. The first method we propose is batch oriented and is ideal for offline tracking. The second is suited for recovering egomotion in large environments where the trajectory of the camera rarely intersects itself and in other situations where many views are necessary to capture the appearance of the scene. The third method is suitable for situations where a few views are sufficient to capture the appearance of the scene, such as object-tracking applications. We demonstrate the techniques on egomotion and head-tracking examples and show that they can track for an indefinite amount of time without accumulating drift.

Key words: Tracking, Drift, View-based appearance models.

1 Introduction

Robust algorithms for estimating the change in the pose of an object from one image to the next are abundant [2, 3, 10, 11, 22, 34]. These pose change estimators are an appealing component for building trackers because they provide a simple layer of abstraction between images and pose, code for them is readily available, they tend to be very robust and accurate. Unfortunately, the classical approaches for building trackers based on these techniques suffer from several problems. One classical approach, sometimes known as differential tracking, accumulates the pose changes between successive pairs of frames to obtain the pose of the object in the current frame. Because each pose change is noisy, the error in the accumulated pose grows over time, and resulting in drift.

An alternative is to simply compute the pose change between each incoming image and the first image in the image sequence. But because pairwise pose change estimation algorithms have limited range, this approach cannot work for arbitrarily large motions. We provide new methods that use these pose-change estimators to build long-range trackers with limited drift.

Our solution generalizes these two classical approaches. Rather than computing pose changes between temporally adjacent frames, or between the current frame and the first frame, our trackers compute pose changes between the current frame and a number of *key frames*, or frames that previously appeared in the image sequence. We show how to merge these pose changes to obtain a pose for the current frame, to update the pose of the key frames, or the trajectory of poses associated with all the frames seen so far.

The resulting trackers have indefinite range, and exhibit bounded drift when tracking in a bounded pose space. Furthermore, these trackers are easy to build, because the pose change estimation algorithm abstracts away details such as the assumed image formation model, the mechanism for computing feature correspondences, and the optimization procedure for registering the images. By updating the pose of the key frames (or of the entire trajectory) our tracker effectively maintains an image-based appearance model of the object to track. This appearance model can later be used to initialize the tracker on subsequent tracking sessions, or can be stitched into a 3D model of the object [17].

We propose three related methods for performing these updates. The first is a batch method, and serves as a good workhorse technique. The second method is an online method well suited to egomotion problems, where capturing the appearance of the scene can require an indefinite number of key frames. This method retains all frames seen so far as candidate key frames, and updates the pose associated with them in sub-linear time. We demonstrate this technique by estimating the pose of a camera rig in a very large environment. The third method is an online method suitable for maintaining the appearance of relatively small objects, such as heads, that fit within the field of view of the camera, and can thus be captured with just a few key frames. This method recovers the pose of the objects and adjusts the pose of key frames using a Kalman update. Because its complexity does not grow over time, this method can track human heads without drift for an indefinite time.

2 Related Work

Our batch algorithms is closely related to the problem of globally consistent registration, such as mosaicking of planar scenes [34,36] and stitching of laser range scans [4, 6, 9, 21, 31, 37, 39]. Our batch method is most similar to the method of Lu and Milios [21], which computes pose differences between pairs of laser range scans, and merges these pose differences into consistent poses by solving a maximum likelihood problem. Other global registration methods take into account additional details about the scans, and so do not use pairwise registration as a subroutine: Stoddart and Hilton [37] attach virtual springs between corresponding points among all pairs of scans and relax the system to convergence. Chen and Medioni [4] rely on a version of the Iterated Closest Point (ICP) algorithm to iteratively compute correspondences and transformations between the scans. Sawhney et al. [34] perform global registration on the overlapping regions of the scans, which are assumed to be of planar structures.

The idea of anchoring tracking against landmarks to reduce drift was exploited in the rigid-body tracking work of Chiuso, Jin, Favaro, and Soatto, [5, 15], who use the pose and appearance of patches to fix a coordinate system. By anchoring the coordinate system against these features when they reappear in the scene, their tracker eliminates the drift incurred from fixing the coordinate system against a poorly estimated feature. Rather than anchoring against 3D patches, our methods anchor against images using a pose change estimator. In [40], the tracker is anchored against static 3D features that are provided to the tracker before hand.

The literature on Simultaneous Localization And Mapping (SLAM) and Structure From Motion (SFM) and adaptive rigid body tracking [1, 5, 7, 13, 15, 18, 19, 24] aims to update an appearance model of the environment (the map) or of an object while simultaneously tracking the pose of the object or of the camera. This body of work tends to differ from ours in that the appearance model is represented as a set of geometric features, such as 3D lines and corners, or as an occupancy grid, rather than as a collection of pose-annotated frames. Updating the model becomes more expensive as more features are introduced into it, so McLauchlan [24] proposed an efficient online update algorithm based on the Kalman filter update that allows certain features to become fixed. Our update algorithm is similar. A notable exception is [14], which captures appearance with a subspace model.

In the SLAM literature, both [38] and [9] represent the map as pose-annotated key frames, as we do. As loops in the trajectory are detected, a propagation step corrects backward poses in the loop. The updates are online, but increase in complexity linearly in the length of the loop in the case of [38] and cubically in the case of [9]. These algorithms are similar in purpose to the algorithm presented in Section 5.

This article is a culmination of our work on building drift-free trackers [28, 32, 33].

3 Tracking Model

As each image becomes available, we compute its pose change with respect to several past key frames using an off-the-shelf pose change estimator. Since these pose changes are a function of the true pose of the object in the corresponding images, we can combine these pose change measurements to update our estimate of the pose of the object throughout the sequence. To do this, we first describe a generative model for pose change estimators, and then describe algorithms for approximating the maximum *a posteriori* (MAP) estimate of the poses.

Let $y_{s,t}$ denote the measured pose change between frames t and s, and let $Y^T = \{y_{s,t}\}_{(s,t)\in\mathcal{O}}$ denote the set of measured pose changes up to time T, stacked vertically into a column vector. Let $X^T = \{x_t\}_{t=1..T}$ be the trajectory of the object from time $t = 1$ to time $t = T$, stacked vertically into a column vector. Finally, let $x_{\mathcal{M}}$ denote the appearance model, which simply consists of the poses of a set of key frames.

We define a prior $p(X^T)$ on the trajectory of poses, and a likelihood $p(Y^T|X^T)$ on the trajectory, and show how to update $p(x_t, x_{\mathcal{M}}|Y^T)$, the posterior distribution over trajectories and the appearance model, as new pose changes become available. This distribution captures our estimate and uncertainty in the pose of the object and the appearance model given all measurements made so far.

3.1 Trajectory Prior $p(X^T)$

We will assume that the object's pose follows *a prior* Markovian dynamics:

$$p(X^T) = p(x_1) \prod_{t=2}^{T} p(x_t|x_{t-1}). \tag{1}$$

The transition density $p(x_t|x_{t-1})$ is a distribution over the state of the object at time t given only its the state at time x_{t-1}. We will assume linear Gaussian dynamics and let the state encode the pose of the object and the derivative of the pose.

For example, define the state $x_t = [\,u_t\ v_t\ \dot{u}_t\ \dot{v}_t\,]^\top$ to be the 2D location and

2D velocity to be tracked. A sensible state-transition model is:

$$x_t = \mathbf{A}x_{t-1} + \omega_t, \tag{2}$$

$$\mathbf{A} = \begin{bmatrix} 1\,0\,1\,0 \\ 0\,1\,0\,1 \\ 0\,0\,1\,0 \\ 0\,0\,0\,1 \end{bmatrix} \tag{3}$$

where ω_t is a zero-mean Gaussian random variable with covariance $\mathbf{\Lambda}_x$. At each time step, this model updates the pose by adding the velocity and some noise to the previous pose, and updates the velocity by adding some random noise to it. Such a model can describe 3D motion by including rotation and angular velocity in the state. The recursive algorithms presented later can operate with nonlinear transition densities of the form $p(x_t|x_{t-1}) = \mathcal{N}(x_t|\mathbf{f}(x_{t-1}), \mathbf{\Lambda}_x)$ by linearizing $\mathbf{f}$ at the current estimate of x_t at each iteration.

Equation (2) can be re-written in the form of Equation (1) as

$$p(x_t|x_{t-1}) = \mathcal{N}(x_t|\mathbf{A}x_{t-1}, \mathbf{\Lambda}_x), \tag{4}$$

where $\mathcal{N}(x|\mu, \mathbf{\Lambda})$ denotes a multivariate Gaussian with mean μ and covariance $\mathbf{\Lambda}$.

3.2 Observation Model $p(Y^T|X^T)$

For certain types of transformations, the ideal pose change $y^*_{s,t}$ between frames at time s and t is additively related to x_s and x_t, so that $x_t = y^*_{s,t} + x_s$. This holds, for example, if the poses represent translations. For other transformations, such as affine, the relationship is multiplicative, so that $\hat{x}_t = \hat{y}^*_{s,t}\hat{x}_s$, where the $\hat{\cdot}$ operator reshapes a vector into a square matrix of the appropriate size ($\mathrm{vec}\,(\cdot)$ is the inverse operation, stacking the elements of a matrix into a column vector). To discuss both types of motion models in one framework, we use the notation $x_t = y^*_{s,t} \oplus x_s$ to describe both operations, and $y^*_{s,t} = x_t \ominus x_s$ to describe the inverse operation. To stay consistent with both multiplication and addition, these operators are associative but not commutative.

Observed pose changes are noisy versions of $x_t \ominus x_s$. The distribution $p(y_{s,t}|x_s, x_t)$ represents the uncertainty in pose-change estimation between two frames at known poses x_s and x_t. Each pose change $y_{s,t}$ is assumed to be mutually

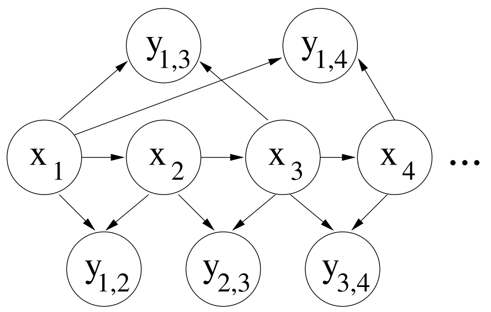

Fig. 1. Independence structure between trajectory and measured pose changes. Each hidden node x_t is the pose associated with a frame. The observed nodes $y_{s,t}$ are measured pose changes as recovered by a registration algorithm.

independent of other pose changes conditioned on x_s and x_t [1]:

$$p(Y^T|X^T) = \prod_{(s,t)\in\mathcal{O}} p(y_{s,t}|x_s, x_t). \tag{5}$$

Figure 1 depicts the independence relationship between poses and pose-change measurements.

To simplify computing the posterior distribution over X^T, we approximate the distribution $p(y_{s,t}|x_s, x_t)$ with a Gaussian, as explained in the appendix:

$$p(y_{s,t}|x_s, x_t) \approx \mathcal{N}(y_{s,t}|y^*, \mathbf{\Lambda}_{s,t}) \tag{6}$$

$$y^* = x_t \ominus x_s \tag{7}$$

$$\mathbf{\Lambda}_{s,t} = \hat{\sigma}^2 \left[\sum_{p\in P} \dot{u}(p, y^*)^\top \nabla I_t(p)^\top \nabla I_t(p) \dot{u}(p, y^*) \right]^{-1} \tag{8}$$

$$\hat{\sigma}^2 = \frac{1}{|\mathcal{P}|} \sum_{i\in\mathcal{P}} \left[I_s(i + u(i, y^*)) - I_t(i) \right]^2, \tag{9}$$

Under this approximation, the mean of the distribution is the true pose change. The covariance is scaled by the reconstruction error $\hat{\sigma}^2$ after warping according to the recovered pose change, and reflects the average sensitivity of the components of the registration model at each pixel by the strength of the image

[1] This independence assumption is a simplification: in general pose change measurements that share a frame are dependent, even when conditioned on the true poses. This is because the random variables $y_{s,t}|x_s, x_t$ and $y_{s,u}|x_s, x_u$ are obtained by registering images, so that $y_{s,t}|x_s, x_t = f(I_s, I_t)$ and $y_{s,u}|x_s, x_u = f(I_s, I_u)$. These images are in turn stochastic functions of the poses. Since $y_{s,t}|x_s, x_t$ and $y_{s,u}|x_s, x_u$ are built from a common random variable I_s, they are dependent on each other. The independence assumption is exact when I_s is a deterministic function of x_s, but in general, this independence assumption results in adequate performance and greatly simplifies the model.

features at that pixel. Equivalently, this can be re-written as

$$y_{s,t} = x_t \ominus x_s + \omega_{s,t}, \tag{10}$$

where $\omega_{s,t}$ is a zero-mean Gaussian with covariance $\mathbf{\Lambda}_{s,t}$.

4 Method 1: Batch

The *a posteriori* most probable trajectory, given measurements Y^T, is defined as

$$X^* = \underset{X^T}{\operatorname{argmax}}\, p(X^T|Y^T) = \underset{X^T}{\operatorname{argmax}}\, p(Y^T|X^T)p(X^T). \tag{11}$$

X^* is the trajectory that is most consistent with the observations Y^T according to the generative model of the previous section.

In the following sections, we show that when the likelihood $p(Y^T|X^T)$ is linear in X^T (for example, when $\ominus$ is a simple difference) and $p(X^T)$ is Gaussian, X^* can be found by solving a sparse linear least-squares problem [21, 33]. When $p(Y^T|X^T)$ is a Gaussian whose mean depends nonlinear on X^T (when $\ominus$ involves matrix inversion), X^* can be found offline by solving a sparse nonlinear least-squares problem.

4.1 Linear-Gaussian Case

When $p(x_t|x_{t-1})$ is Gaussian and linear in x_{t-1} (for example, see Equation (4)), X^T is a zero-mean Gaussian random variable with

$$p(X^T) \propto \exp\left(-\left(X^T\right)^\top \mathbf{\Lambda}_X^{-1} X^T\right), \tag{12}$$

with the inverse covariance $\mathbf{\Lambda}_X^{-1}$ block tri-diagonal.

If the relationship between observation $y_{s,t}$ and x_s and x_t is additive, Equation (7) becomes:

$$y^*_{s,t} = \mathbf{C}x_t - \mathbf{C}x_s = \mathbf{C}_{s,t}X^T \tag{13}$$

$$\mathbf{C}_{s,t} = \begin{bmatrix} 0 \cdots & -\mathbf{C} \cdots & 0 \cdots & \mathbf{C} \cdots \end{bmatrix}, \tag{14}$$

The matrix $\mathbf{C}$ extracts the pose components of the state x_t, so that, for example, if $x_t = [\,u_t\ v_t\ \dot{u}_t\ \dot{v}_t\,]^\top$, then $\mathbf{C}x_t = [\,u_t\ v_t\,]^\top$. The matrix $\mathbf{C}_{s,t}$ has $-\mathbf{C}$ at the location corresponding to s, $\mathbf{C}$ at the location corresponding to t, and $\mathbf{0}$ elsewhere.

Stacking up the $\mathbf{C}_{s,t}$ into $\mathcal{C}$ and $\mathbf{\Lambda}_{s,t}$ into $\mathbf{\Lambda}_{Y|X}$ gives the likelihood

$$p(Y^T|X^T) = \mathcal{N}\left(Y^T \middle| \mathcal{C}X^T, \mathbf{\Lambda}_{Y|X}\right). \tag{15}$$

This linear-Gaussian likelihood, in conjunction with the Gaussian prior (12) gives a Gaussian posterior $p(X^T|Y^T)$ over X^T. The covariance $\mathbf{\Lambda}_{X|Y}$ and the mean $m_{X|Y}$ of this posterior can be obtained by solving these two equations [30]:

$$\mathbf{\Lambda}_{X|Y}^{-1} = \mathbf{\Lambda}_X^{-1} + \mathcal{C}^\top \mathbf{\Lambda}_{Y|X}^{-1} \mathcal{C} \tag{16}$$

$$\mathbf{\Lambda}_{X|Y}^{-1} m_{X|Y} = \mathcal{C}^\top \mathbf{\Lambda}_{Y|X}^{-1} Y^T. \tag{17}$$

When there are T trajectory steps and $|\mathcal{O}|$ observations, this computation can take $O(T^3)$ if performed naively. Using the conjugate gradient method, Equation (17) can be solved in $O(T(T + |\mathcal{O}|))$: T iterations, each requiring a matrix multiplication that takes time proportional to the number of nonzero elements in $\mathbf{\Lambda}_{X|Y}^{-1}$.

4.2 Nonlinear Case

When Equation (7) relates $y_{s,t}$ nonlinearly with x_t and x_s, we can linearize the relationship and apply the batch method of the previous section. The batch solution provides a new point about which to linearize the relationship, and the process is repeated.

In the case of affine transformations, for example, a first order Taylor series approximation of Equation (7) about $\hat{\hat{x}}_t$ and $\hat{\hat{x}}_s$ gives [26]:

$$x_t \ominus x_s = \hat{x}_t \hat{x}_s^{-1} \approx \operatorname{vec}\left(\hat{\hat{x}}_t \hat{\hat{x}}_s^{-1}\right) + d\left(\hat{\hat{x}}_t \hat{\hat{x}}_s^{-1}\right) \tag{18}$$

$$d\left(\hat{\hat{x}}_t \hat{\hat{x}}_s^{-1}\right) = (d\hat{\hat{x}}_t)\hat{\hat{x}}_s^{-1} + \hat{\hat{x}}_t d(\hat{\hat{x}}_s^{-1}) = (d\hat{\hat{x}}_t)\hat{\hat{x}}_s^{-1} - \hat{\hat{x}}_t \hat{\hat{x}}_s^{-1}(d\hat{\hat{x}}_s)\hat{\hat{x}}_s^{-1} \tag{19}$$

$$d\hat{\hat{x}}_s = \hat{x}_s - \hat{\hat{x}}_s \tag{20}$$

$$d\hat{\hat{x}}_t = \hat{x}_t - \hat{\hat{x}}_t. \tag{21}$$

Substituting terms, and applying the identity $\operatorname{vec}(\mathbf{ABC}) = (\mathbf{C}^\top \otimes \mathbf{A})\operatorname{vec}(\mathbf{B})$, where $\otimes$ is the Kronecker product [26], yields

$$y_{s,t}^* - \operatorname{vec}\left(\hat{\hat{x}}_t \hat{\hat{x}}_s^{-1}\right) = \left(\hat{\hat{x}}_s^{-\top} \otimes \mathbf{I}\right) x_t - \left(\hat{\hat{x}}_s^{-\top} \otimes \hat{\hat{x}}_t \hat{\hat{x}}_s^{-1}\right) x_s, \tag{22}$$

where $\mathbf{I}$ is the identity matrix. This relationship is now in the form of Equation (13) and the method of the previous section can be applied.

Once the optimal X_s and X_t are found, the system is linearized again as per Equation (22) and the operation is repeated.

4.3 Selecting Pairs of Frames

Image registration is the main computational bottleneck of the batch method. In practice, it is costly to compute the pose change between every pair of frame (s, t), so $\mathcal{O}$ must be chosen with some discretion. In addition, registration algorithms work most reliably if the motion between the two views is small. For example, when tracking a head, the 6-degrees-of-freedom registration algorithm we use in our experiments returns a reliable pose estimate if the head has undergone a rotation of at most 10 degrees along any axis.

So we seek frame pairs (s, t) that yield high-quality registration (as quantified by the trace of $\mathbf{\Lambda}_{s,t}$) without actually performing registration on every pair of images. To identify such frame pairs, we search for pairs of images that are similar according to their sum of squared differences (SSD). If the SSD between frames s and t is within threshold, (s, t) is inserted into $\mathcal{O}$ and $y_{s,t}$ is computed using the registration algorithm.

5 Method 2: Online Updates.

In online tracking pose changes must be incorporated into the estimate of the trajectory X^T as soon as a new frame becomes available. We show an efficient way to approximately update X^T with pose change measurements as they become available. Rather than re-running the batch algorithm of the previous section each time, we propose simplifying the correlation between the pose estimates to allow measurements to be incorporated in linear-time.

A new measurements is independent of past measurements conditioned on X^T, so the maximum *a posterior* X^T can be updated recursively as follows:

$$\max_{X^T} p(X^T|Y^T) = \max_{X^T} p(X^T|Y^{T-1}, y_{s,t}) = \max_{X^T} p(y_{s,t}|X^T)p(X^T|Y^{T-1}). \quad (23)$$

This update uses $p(X^T|Y^{t-1})$ as a prior, and $p(y_{s,t}|X^T)$ as a likelihood. When $p(y_{s,t}|X^T)$ is linear and Gaussian (see (13)), and $p(X^T|Y^{T-1}$ has covariance $\mathbf{\Lambda}_X$, the posterior over X^T can again be obtained in closed form by solving $\mathbf{\Lambda}_{X|Y}$ and $m_{X|Y}$ [30]:

$$\mathbf{\Lambda}_{X|Y}^{-1} = \mathbf{\Lambda}_X^{-1} + \mathbf{C}_{s,t}^{\top} (\mathbf{\Lambda}_{s,t})^{-1} \mathbf{C}_{s,t} \quad (24)$$

$$\mathbf{\Lambda}_{X|Y}^{-1} m_{X|Y} = \mathbf{C}_{s,t}^{\top} (\mathbf{\Lambda}_{s,t})^{-1} y_{s,t}. \quad (25)$$

Solving for $m_{X|Y}$ using conjugate gradient takes $O(T^2 + T|\mathcal{O}|)$. That is, incorporating a single $y_{s,t}$ takes as much work as incorporating all of Y^T all at once! Our solution is to approximate $\mathbf{\Lambda}_X$ by a tri-diagonal matrix. This makes $\mathbf{\Lambda}_{X|Y}^{-1}$

invertible in time linear in T using forward-backward substitution, allowing us to incorporate new measurements in time $O(T)$.

In this section, we present a method for simplifying $\Lambda_{X|Y}^{-1}$ to block tri-diagonal form after each measurement is inserted. For Gaussian variables, a block tri-diagonal covariance matrix corresponds to a Markovian independence structure. With minor adaptation, the method presented here can simplify $\Lambda_{X|Y}^{-1}$ to any tree structure, but the tri-diagonal or Markov structure is appealing because it is the simplest structure that allows the influence of measurements to propagate throughout the entire trajectory X^T, allowing loops to be closed and resulting in smooth trajectories. Intuitively, a Markov structure imposed between the poses of chronologically adjacent frames expresses the prior knowledge that frames that are observed near the same time should have similar poses. We demonstrate in Section 7.1 that a simpler structure such as a diagonal matrix, which does not allow for such propagation, does not result in smooth trajectories. In general, after incorporating each measurement, the independence structure of $p(X^T|Y^T)$ is simplified into a Markov chain, which simplifies the incorporation of the next measurement to $O(T)$ in the worst case, and to a small constant in practice.

The approximation strategy follows the pattern of Assumed Density Filtering (ADF) [25]: at each iteration, $p(X^T|Y^{T-1})$ is approximated with a simpler distribution $q(X^T)$ that factors as a Markov chain. To incorporate a new measurement $y_{s,t}$, we apply Bayes rule with $q(X^T)$ as a prior and $p(y_{s,t}|x_s, x_t)$ as likelihood:

$$p(X^T|Y^T) \propto p(y_{s,t}|x_s, x_t)q(X^T). \tag{26}$$

To incorporate the next measurement, $p(X^T|Y^T)$ is again approximated with a simpler distribution, and the process is repeated. Figure 2 summarizes this process.

In the linear-Gaussian case, it is possible to compute in $O(T)$ a Gaussian approximation $q(X^T)$ with minimum Kullback-Leibler divergence to $p(X^T|Y^{T-1})$. One way to do this is to invoke tools for covariance extension (see, for example, [16, 20]). The remainder of this section describes our variant of these techniques, which is formulated as a two-pass message-passing algorithm on a loop. This approach is particularly well suited for this problem because messages need not be propagated beyond a node if the influence of the message on the node is small. This allows early termination of the algorithm, allowing it to take time sub-linear in T.

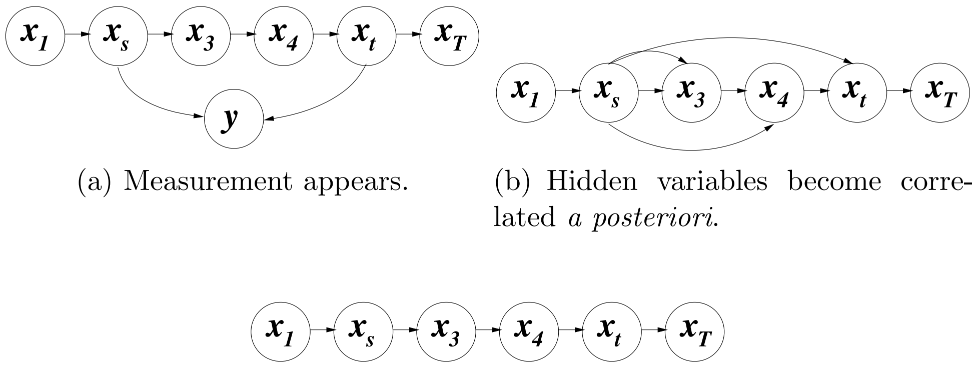

(a) Measurement appears.

(b) Hidden variables become correlated *a posteriori*.

(c) The correlation structure is approximated to allow new measurements to be incorporated easily.

Fig. 2. Using Assumed Density Filtering to maintain a Markov approximation to the correlation induced by measurements on the trajectory.

5.1 Updating the Trajectory

We would like to approximate an arbitrary distribution that factors according to $p(X) = \prod_t p_t(x_t|\text{Pa}[x_t])$, with one that factors according to the Markov property $q(X) = \prod_t q_t(x_t|x_{t-1})$. Here, $\text{Pa}[x_t]$ are the parents of node x_t in the graph prescribed by the factorization of $p(X)$. In Appendix B, we show that the distribution q that is closest to p according to the Kullback-Leibler divergence is

$$q_t(x_t|x_{t-1}) = p(x_t|x_{t-1}). \tag{27}$$

So the best conditional q_t is built up from the conditional marginals of p. Computing each q_t in a graph is generally an expensive operation, but in a graph with a single loop, it can be done in time proportional to the number of nodes in the graph.

Instead of first computing $p(X^T|Y^T)$ and then simplifying it onto a suitable $q(X^T)$, we compute q directly from $p(X^T|Y^{T-1})$. We have just shown that this q factors into conditional distributions $q_t(x_t|x_{t-1}) = p(x_t|x_{t-1}, y_{s,t}, Y^{T-1})$. These factors are computed differently depending on their location in the graph. In what follows, we omit the dependence on Y^{T-1} for brevity, and assume that all distributions are conditioned on Y^{T-1}.

5.1.1 Finding $p(x_\tau|x_{\tau-1}, y_{s,t})$ for $s < \tau < t$

Because for every $s < \tau < t$, $p(x_\tau|x_{\tau-1}, x_t) = p(x_\tau|x_{\tau-1}, x_t, y_{s,t})$ (see Figure 2), we have

$$p(y_{s,t}, x_{\tau-1}, x_\tau, x_t) = p(y_{s,t}, x_{\tau-1}, x_t)p(x_\tau|x_{\tau-1}, x_t) \tag{28}$$

We can find $p(x_\tau|x_{\tau-1}, y)$ by marginalizing out x_t from $p(y_{s,t}, x_{\tau-1}, x_\tau, x_t)$ and normalizing. We can also find $p(x_\tau|y)$ by marginalizing out both x_t and $x_{\tau-1}$ and normalizing. Finally, we can compute $p(y, x_\tau, x_t)$ for the next τ in the iteration.

There are two missing pieces for computing $p(y_{s,t}, x_{\tau-1}, x_\tau, x_t)$: The first is $p(y_{s,t}, x_s, x_t) = p(y_{s,t}|x_s, x_t)p(x_s, x_t)$ for starting the recursion. $p(y|x_s, x_t)$ is the given measurement model, and $p(x_s, x_t)$ can be obtained by marginalizing over $p(X^T)$. The second missing piece is $p(x_\tau|x_{\tau-1}, x_t)$. Note that this quantity does not depend on the measurements and could be computed offline. The recursion for calculating it is:

$$p(x_\tau|x_{\tau-1}, x_t) \propto p(x_t|x_\tau)p(x_\tau|x_{\tau-1}) \tag{29}$$
$$p(x_t|x_\tau) = \int \mathbf{d}x_{\tau+1}\, p(x_t|x_{\tau+1})p(x_{\tau+1}|x_\tau) \tag{30}$$

The second equation describes a recursion that starts from t and goes down to s. It computes the influence of node τ on node t. Equation (29) is coupled to this recursion and uses its output. Because this recursion runs in the opposite direction of the recursion described by (28), $p(x_\tau|x_{\tau-1}, x_t)$ has to be computed in a separate pass.

The forward and backward recursions visit every element of the chain once. To speed up computation, we stop a recursion in either direction when it does not modify the value of the current node significantly. This is an acceptable stopping criterion because a small change in a node guarantees that the iterations will not modify subsequent nodes significantly.

5.1.2 Finding $p(x_\tau|x_{\tau-1}, y_{s,t})$ *for* $1 \le \tau \le s$

Starting from $\tau = s - 1$, compute

$$p(y_{s,t}|x_\tau) = \int \mathbf{d}x_{\tau+1}\, p(y_{s,t}|x_{\tau+1})p(x_{\tau+1}|x_\tau) \tag{31}$$
$$p(x_\tau|y_{s,t}) \propto p(y_{s,t}|x_\tau)p(x_\tau) \tag{32}$$
$$p(x_\tau|x_{\tau-1}, y_{s,t}) \propto p(y_{s,t}|x_\tau)p(x_\tau|x_{\tau-1}) \tag{33}$$

The recursion first computes the influence of x_τ on the observation, then computes the marginal and the transition probability.

5.1.3 Finding $p(x_\tau|x_{\tau-1}, y_{s,t})$ for $t \leq \tau \leq T$

Starting from $\tau = t$, compute

$$p(x_\tau|y_{s,t}) = \int \mathbf{d}x_{\tau-1}\, p(x_\tau|x_{\tau-1}, y_{s,t})p(x_{\tau-1}|y_{s,t}) \quad (34)$$

$$p(x_\tau|x_{\tau-1}, y_{s,t}) = p(x_\tau|x_{\tau-1}). \quad (35)$$

The second identity follows from the independence structure on the right side of observed nodes.

To handle nonlinear observations, one can again linearize the observation equation, as in Section 4.2. If so desired, after running the operation described in this section, the procedure may be repeated to yield a better answer. In this way, the procedure described here serves as an approximate Newton step.

5.2 Selecting Frame Pairs

At each time step t, the online algorithm must determine the set of frames $s < t$ to register against the frame at time t. Picking frames whose appearance is similar to the current frame works well if there is a one-to-one mapping between appearance and pose. But in some situations, for example objects with repetitive texture such as floor tiles or a calibration cube with identical sides, different poses yield the same appearance. To disambiguate between these situations, key frames that sufficiently resemble the current frame in appearance are registered only if their pose is likely to be within tracking range of each other.

To assess the probability that the pose x_s of a potential base frame is within tracking range of the pose x_t of the current frame, we compute the probability that $|x_s - x_t|$ is above some tracking range Δx. If this probability is above a threshold, then the two frames are deemed likely to be close in pose and $y_{s,t}$ is measured. This probability can be estimated by evaluating

$$\int_{|x_s - x_t| \leq \Delta x} p(x_s, x_t|Y^{T-1}, y_{t-1,t})\, dx_s dx_t, \quad (36)$$

which is the probability that x_s and x_t are within tracking range given all measurements prior to measuring the pose change between s an t. The mean and covariance of $p(x_s, x_t|Y^{T-1}, y_{t-1,t})$ can be read from the parameters of $p(X^T|Y^{T-1}, y_{t-1,t})$. Equation (36) can be quickly approximated by Monte Carlo by drawing samples (x_s, x_t) from $p(x_s, x_t|Y^{T-1}, y_{t-1,t})$ and reporting the ratio of samples where $|x_s - x_t| \leq \Delta x$ to the total number of samples drawn.

6 Method 3: Sparse key frames.

For some tracking applications, only a few key frames are needed to capture the appearance of the scene. In these cases, instead of updating the entire trajectory, we update the pose of the current frame and of a few key frames only. The pose of these frames is maintained as a state vector using a Kalman filter, but during the prediction step, the filter removes old elements or inserts new elements in the state vector as needed. The update step of the Kalman filter incorporates new measurements. The resulting filter has a computational complexity that grows cubically in the size of the state vector, so in practice we limit the number of key frames to about 50.

At time t, the tracker maintains a Gaussian distribution $p(x_t, x_{\mathcal{M}}|Y^T)$ over the pose of the current frame and the poses $x_{\mathcal{M}} = \{x_{M_1}, x_{M_2}, \cdots\}$ of the key frames. Define the variable $\mathcal{X}$ as the vertical concatenation x_t and $x_{\mathcal{M}}$:

$$\mathcal{X} = \Big[x_t \ ; \ x_{M_1} \ ; \ x_{M_2} \ ; \ \ldots\Big]. \tag{37}$$

The tracker need only maintain the mean $m_{\mathcal{X}}$ and covariance $\mathbf{\Lambda}_{\mathcal{X}}$ of $p(\mathcal{X}|Y^T)$. To incorporate a new measurement $y_{s,t}$, the tracker applies a Kalman update to $p(\mathcal{X}|Y^{T-1})$ to obtain $p(\mathcal{X}|Y^{T-1}, y_{s,t})$. After all pairwise measurements involving frame t have been performed, the tracker turns x_t into a key frame, and may decide to evict one of the older key frames. Then the tracker must prepare to incorporate pose change estimates involving a new frame at time $t + 1$. We examine each step separately.

6.1 Incorporating a new measurement

In the linear case, as before, incorporating $y_{s,t}$ with the prior $p(\mathcal{X}|Y^T)$ gives a Gaussian $p(\mathcal{X}|Y^T, y_{s,t})$ whose mean and covariance can be obtained by solving for $m^{new}_{X|Y}$ and $\mathbf{\Lambda}^{new}_{X|Y}$ in

$$[\mathbf{\Lambda}^{new}_{\mathcal{X}}]^{-1} = [\mathbf{\Lambda}_{\mathcal{X}}]^{-1} + \mathbf{C}^{\top}_{s,t}\mathbf{\Lambda}^{-1}_{s,t}\mathbf{C}_{s,t} \tag{38}$$

$$[\mathbf{\Lambda}^{new}_{\mathcal{X}}]^{-1} m^{new}_{\mathcal{X}} = [\mathbf{\Lambda}_{\mathcal{X}}]^{-1} m_{\mathcal{X}} + \mathbf{C}^{\top}_{s,t}\mathbf{\Lambda}^{-1}_{s,t}\ y_{s,t}. \tag{39}$$

The main computational burden in introducing a new measurement is solving for $m^{new}_{\mathcal{X}}$ in Equation (39). $[\mathbf{\Lambda}^{new}_{\mathcal{X}}]^{-1}$ will be dense after a few measurements, so solving the linear system takes cubic time in the number of key frames. We can bound the complexity of this updated by capping the number of key frames. When pose change measurements are nonlinearly related to poses, the relationship can be linearized prior to applying Equations (38) and (39) using Equation (22).

6.2 Preparing for a new frame

After incorporating all pose changes relating to frame t, the frame at time t becomes a key frame, and the mean and covariance of $\mathcal{X}$ are augmented to make room for the pose x_{t+1}, to represent the distribution $p(x_{t+1}, x_t, x_{\mathcal{M}}|Y^T)$. If we have no *a priori* information about the pose x_{t+1}, we simply set the corresponding entry in the inverse covariance to 0. This translates to infinite marginal variance on x_{t+1}:

$$m_{\mathcal{X}}^{aug} = \begin{bmatrix} 0 \; ; \; m_{\mathcal{X}} \end{bmatrix} \tag{40}$$

$$[\mathbf{\Lambda}_{\mathcal{X}}^{aug}]^{-1} = \begin{bmatrix} 0 & 0 \\ 0 & \left[\Lambda_{\mathcal{X}}^{old}\right]^{-1} \end{bmatrix}. \tag{41}$$

Since the augmented blocks of $\mathbf{\Lambda}_{\mathcal{X}}$ are 0, we have assumed that *a priori*, x_{t+1} is independent of x_t. If there is side knowledge about dynamics, it can be incorporated in this step.

6.3 Evicting old key frames

When a key frame is no longer needed, it is marginalized out of the distribution $p(\mathcal{X}|Y^T)$. This is accomplished by removing the corresponding elements of $m_{\mathcal{X}}$ and the corresponding rows and columns from $\mathbf{\Lambda}_{\mathcal{X}}$.

In our tracker, a frame $t-1$ is always used as a base frame for frame t. Often, this frame is eliminated from the key frame set after estimating its pose change with frame t. In addition, older key frames are sometimes dropped to make room for key frames corresponding to poses that are more commonly visited.

6.4 Picking good key frames

To populate the key frames, we seek frames with accurate pose estimates and that capture representative views of the object. After estimating the pose of the current frame, the tracker determines whether the previous frame should become a key frame. A key frame should be available whenever the object returns near a previously visited pose. To identify poses that the object is likely to revisit, the pose-space is tessellated into adjacent regions, each region maintaining a key frame. A key frame is assigned to a region if it can be ascertained that the pose of the key frame falls within the region with high probability.

The probability that x_{t-1} belongs to a region centered at x_r is:

$$\Pr[x_{t-1} \in B(x_r)] = \int_{x \in B(x_r)} \mathcal{N}(x|E[x_{t-1}], \Lambda_{t-1}) dx, \tag{42}$$

where $B(x)$ is the region centered around a location x, and $E[x_{t-1}]$ and Λ_{t-1} can be read from $m_{\mathcal{X}}^{new}$ and $\Lambda_{\mathcal{X}}^{new}$.

If frame x_{t-1} belongs to a region with higher probability than any other frame so far, it is deemed the best representative for that region, and it is assigned to that region. If the pose does not belong to any region with sufficiently high probability, or all regions already maintain key frames with higher probability, the frame is discarded.

These criteria exhibit several desirable properties: 1) Frames are assigned to regions near their estimated pose. 2) Frames with low certainty in their pose do not become key frames, because the integral of a Gaussian under a fixed volume decreases with the variance of the Gaussian. 3) key frames are replaced when better key frames are found for a given region.

7 Experiments

The online algorithm of Section 6 is well-suited for scenes or objects whose appearance can be captured with a few key frames. We apply it to a face tracking application that uses stereo cameras. The algorithm of Section 5 retains the pose of all frames seen so far, and is well suited for situations where the appearance of the scene or object cannot be well captured with a few frames. We demonstrate it on an egomotion experiment in an large environment whose appearance requires many views to capture. Since the batch algorithm of Section 4 can also potentially use all frames as key frames, we compare it against the online algorithm of Section 5 to evaluate the quality of the Markov chain simplification the latter performs.

7.1 Egomotion in a room.

To demonstrate the online algorithm of Section 5, we manually maneuvered a monocular camera rig inside a large environment and attempted to recover the location of the camera. The camera faced upward and observed its motion relative to the ceiling. The excursions were about three minutes long, producing about 6000 frames of data for each experiment. The trajectory was marked on the floor before the experiment so we could revisit specific locations (see the schematics of Figures 3 and 5). This was done to make the evaluation of the results simpler. The trajectory estimation worked at frame rate for the duration of both trajectories, although it was processed offline to simplify data acquisition.

In these experiments, the pose parameters were (x, y) locations on the floor. All experiments assume the motion dynamics detailed in Section 3.1. For each new frame, pose changes were computed with respect to at most three base frames. The selection of base frames was based on a comparison of the appearances of the current frame and all past frames. The pose-change estimator was a Lucas-Kanade optical flow tracker [23]. To compute pose displacements, we computed a robust average of the flow vectors using an iterative outlier rejection scheme. We used the number of inlier flow vectors as a crude estimate of the precision of $p(y_{s,t}|x_s, x_t)$.

Figures 3 and 5 compare the algorithm of Section 5 against three others: a naive differential tracker that accumulates the pose change between adjacent frames, the batch approach of Section 4, and a variant of the online method of Section 4 that projects the covariance matrix to a fully factorized form after incorporating each pose change. Figure 4 plots the distance between the location recovered the batch method and each of the three algorithms. Although our recovered trajectories do not coincide exactly with the batch solutions, ours are smooth and consistent.

In contrast, more naive methods of reconstructing trajectories do not exhibit these two desiderata. Estimating the motion of each frame with respect to only the previous base frame yields an unsmooth trajectory. Furthermore, loops can not be closed correctly (for example, the robot is not found to return to the origin).

Projecting the correlation structure to a fully factored form is a very simple way of taking into account multiple base frames. This corresponds to using a diagonal matrix to represent the correlation between the poses (instead of the tri-diagonal inverse covariance matrix our algorithm uses). This method also fails to meet our requirements: the resulting trajectory is not smooth, and loops are not closed well.

The trajectories were each about 2000 frames long. The computational complexity of the online algorithm of 5 is linear in the number of frames in the worst case, but thanks to the stopping criterion of the algorithm, the first and last frames both about 5 ms to incorporate (MATLAB code on a 1.2 Ghz PIII), while incorporating a loop closure took about 20 ms.

By taking into account a minimum amount of correlation between frame poses, loops have been closed correctly and the trajectory is correctly found to be smooth.

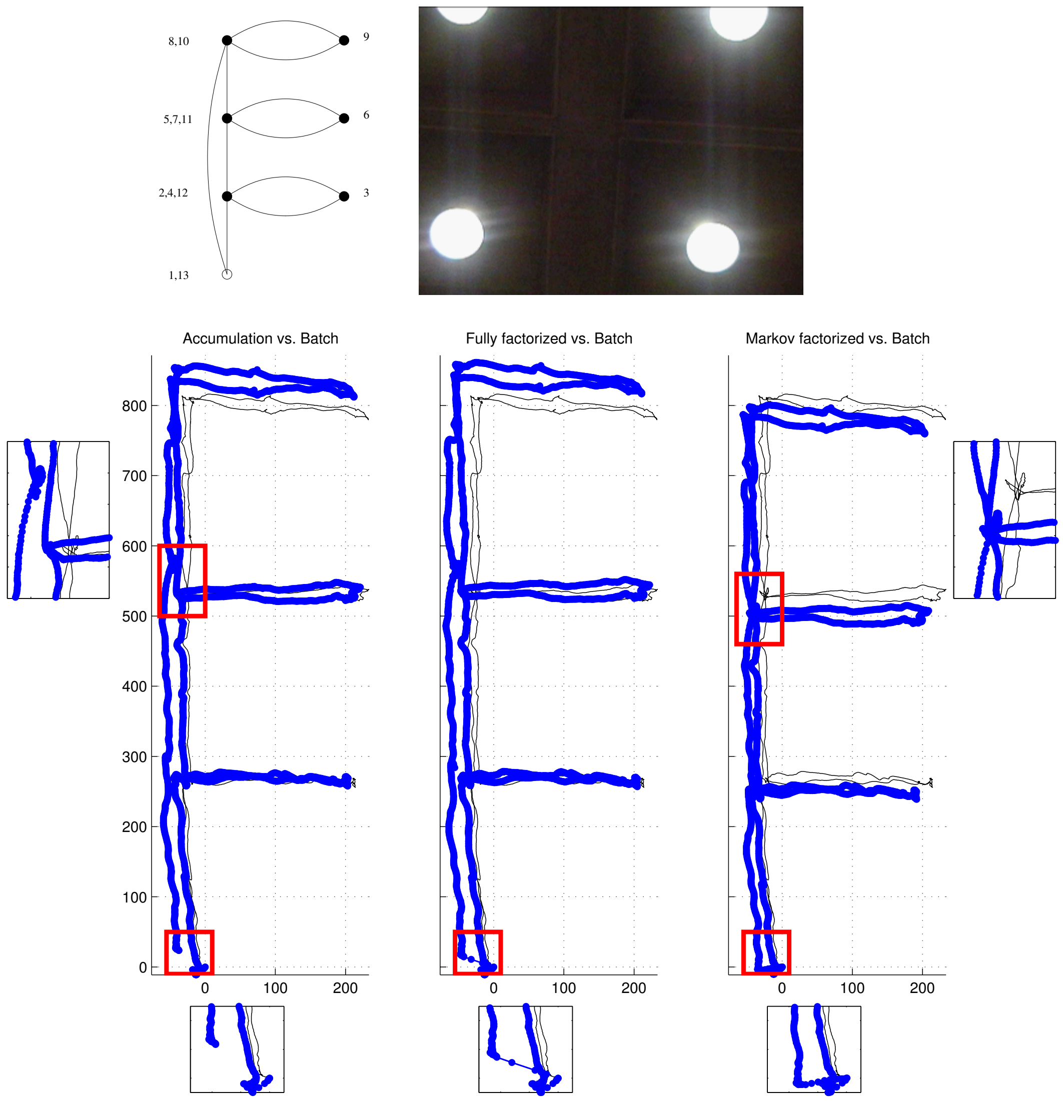

Fig. 3. Recovered trajectories from egomotion experiments. Axes are labeled in centimeters. The camera smoothly followed the trajectory shown in the schematic on the upper left, visiting the waypoints in the order specified by the numbers, starting with waypoint 1. The image in the upper right shows a typical snapshot of the ceiling. The bottom left panel compares the trajectory recovered by accumulating pose changes between successive frames (thick dotted path) to the batch solution of Section 4 (solid path). Loops are not closed well (bottom and left insets). The middle panel compares the trajectory recovered by fully factorizing the covariance after incorporating each measurement (dotted path) and the batch solution (solid path). Loops are closed abruptly, resulting in large jumps in the trajectory (bottom inset). The right panel compares the algorithm of Section 5 to the batch solution. Loops are closed, and the trajectory is smooth. The average distance between pose estimates between the batch solution and each online algorithm was 27 cm for naive accumulation, 26 cm for the fully factorized solution, and 23 cm for the Markov factorization solution.

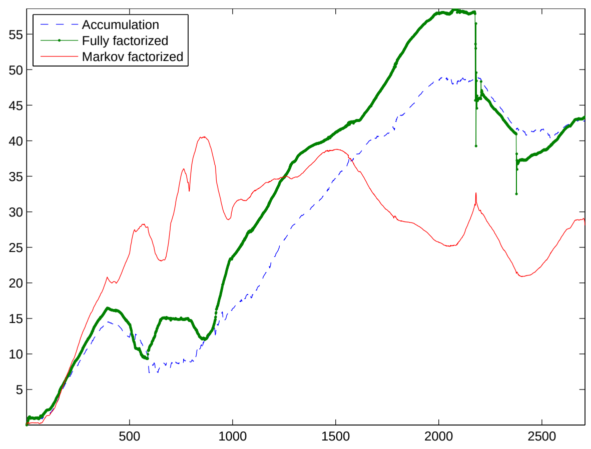

Fig. 4. The distance between the batch algorithm and the three other algorithms. While the Markov factorization method exhibits some shrinkage early in the sequence, it overtakes the other two algorithms later on.

7.2 Key-frame-based 6-DOF Stereo Tracking.

In this experiment, we qualitatively compare three approaches for head-pose tracking: differential tracking, tracking using the first and previous frames as key frames, and the algorithm of Section 6. All three approaches use a 6-DOF (degree-of-freedom) registration algorithm (described in [27] and in the following subsection) to track and create an appearance model of a head undergoing large movements in the near field (approximately one meter from the camera) for several minutes. The camera system is a Videre Design stereo camera pair [41] that delivers depth and intensity maps in real time. In the second experiment, we present a quantitative analysis of our view-based tracking approach by comparing it with the *Inertia Cube*^{2} inertial sensor.

7.2.1 6-DOF Registration Algorithm

At each time step, the camera system provides an intensity image I_t and a depth image Z_t. Given frames (I_t, Z_t) and (I_s, Z_s), the registration algorithm estimates a 6-DOF (3 rotation using the twist parameterization [29] and 3 translation parameters) pose change $y_{s,t}$ between these frames. It first identifies the object of interest by assuming that it is the front-most object in the scene, as determined by the range images Z_s and Z_t. For both frames, the foreground pixels are grouped into a connected component, and the background is masked out. The registration parameters are computed in several steps: First the centers of mass of the regions of interest are aligned in 3D translation. This provides a good starting point for aligning the images using 2D cross-correlation in the image plane. The output of this alignment provides a good initialization point for a finer-grained registration algorithm based on Iterative Closest Point (ICP) and the Brightness Constancy Constraint Equation

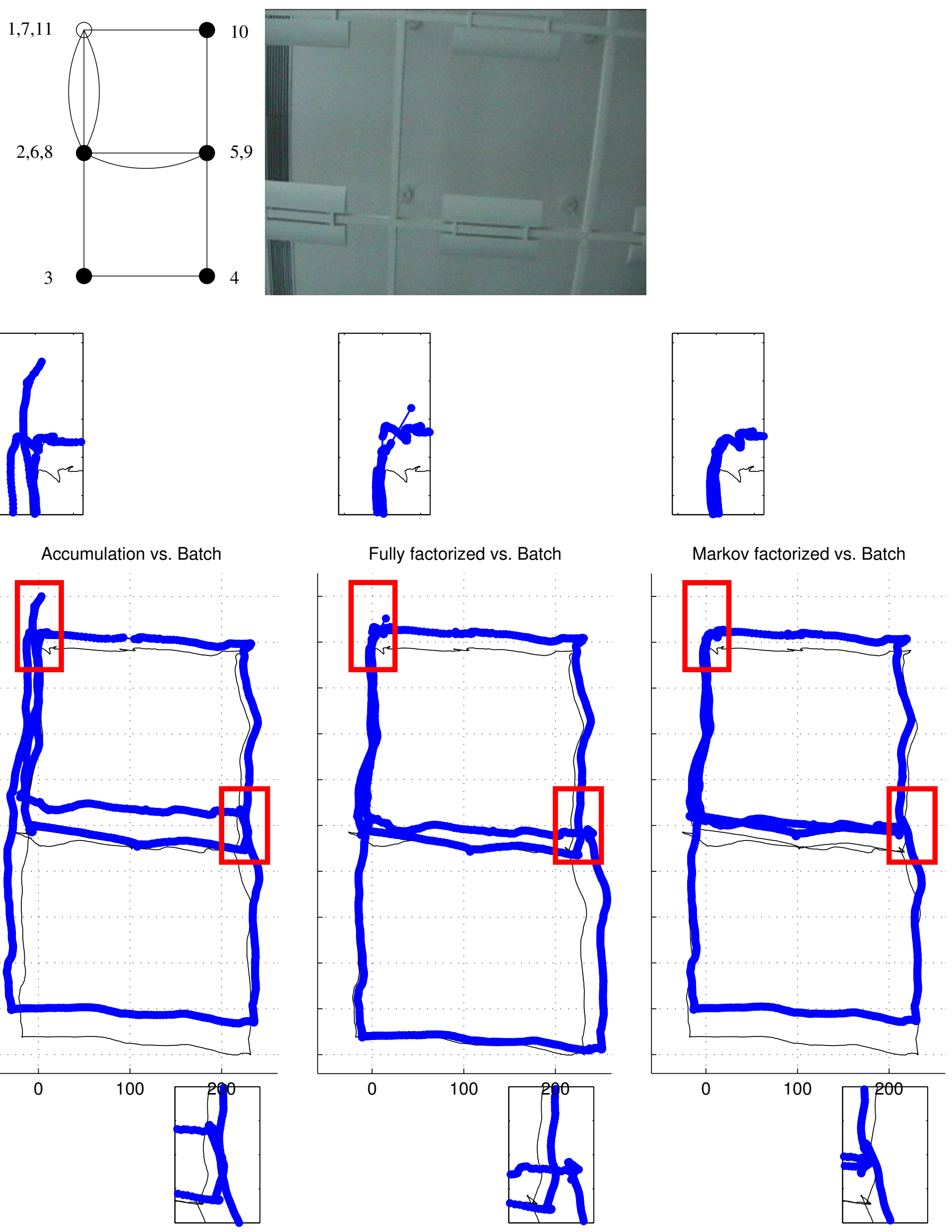

Fig. 5. See caption of Figure 3 for the setup. Naive accumulation does not close loops well, full factorization results in abrupt jumps in the trajectory, and the Markov factorization results in smooth trajectories that close loops well. The average distance between pose estimates between the batch solution and each online algorithm was 26 cm for naive accumulation, 18 cm for the fully factorized solution, and 12 cm for the Markov factorization solution.

(BCCE).

The ICP algorithm iteratively computes correspondences between points in the depth images and finds the 6-DOF transformation parameters that minimize the distance between these pixels. By using depth values obtained from the range images, the BCCE can also be used to recover 3D pose-change estimates [10]. We have found that the BCCE provides superior performance in estimating rotations, whereas ICP provides more accurate translation estimates.

The registration technique of [27] minimizes the sum of the objective functions of ICP and BCCE iteratively, taking advantage of the strengths of both algorithms. At each step of the minimization, correspondences are computed for building the ICP cost function. Then the ICP and BCCE cost functions are linearized, and the locally optimal solution is found using a robust least-squares solver [12]. This process usually converges within 3 to 4 iterations. For more details, see [27].

7.2.2 Head-Pose Tracking

We tested our view-based approach with sequences recorded at 5 Hz. The tracking was performed using the method of Section 6. The pose space used for acquiring the view-based model was evenly tessellated in rotation only. On a 1.7 GHz Pentium 4, our C++ implementation of the tracking framework, including frame grabbing, 3D-view registration, and pose updates, runs at 7 Hz.

Tracking requires no manual intervention: the tracker searches for a frontal face in the scene using a face detector [42]. Because the face is frontal, we use this first frame to establish the origin. The system begins with no key frames, so accurate tracking in the early stages requires the user to move slowly. As more key frames are acquired, the system becomes robust to very fast movements. During steady state, the head tracker maintains about 50 key frames.

Figure 6 shows tracking results from a video sequence in which the subject underwent rotations of about 110 degrees and translations of about 80 cm, including translation along the Z-axis. While this sequence was 2 minutes long, in practice, tracking can continue indefinitely under these conditions. We have run experiments where the tracker was stable for 30 minutes, limited only by the patience of the subject. The tracker is tolerant of most hazards, including lighting variations and occlusions, as long as the segmentation algorithm provides good foreground pixels. In the current implementation, the segmentation algorithm simply returns pixels near the camera, so intervening objects can interfere with tracking. The left column of Figure 6 shows that a differential tracker based on our pose-change estimation algorithm drifts after a short while on this sequence. When tracking with only the first and previous frames as key frames (center column), the pose estimate is accurate when the subject is near-frontal but drifts when moving outside this region. The view-based approach (right column) gives accurate poses during the entire the sequence

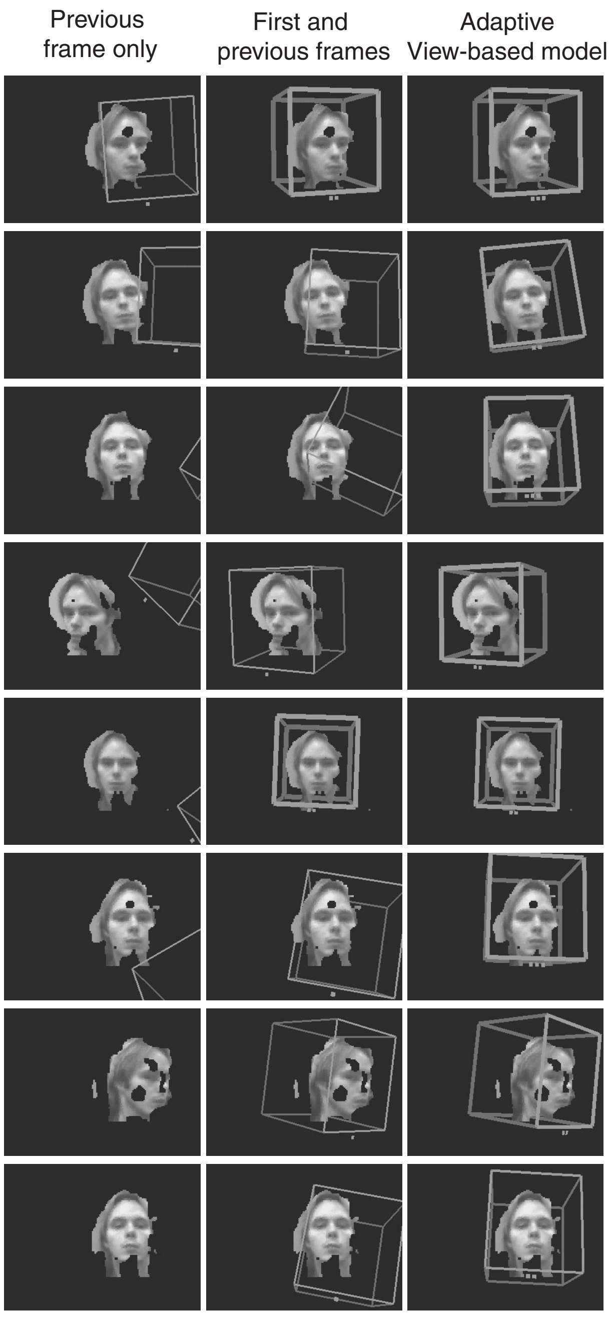

Fig. 6. Comparison of face tracking results using a 6-DOF registration algorithm. Rows represent results at 31.4, 52.2, 65, 72.6, 80, 88.4, 113, and 127 seconds into the video. Each image shows the foreground pixels and a rendered cube representing the pose of the head. The thickness of the lines defining the box around each face is inversely proportional to the uncertainty in the pose estimate (the determinant of the covariance of x_t, read from $\Lambda_{\mathcal{X}}$). The number of indicator squares below the box indicate the number of base frames used during tracking. Background pixels and pixels where no range data was available are shown in black. Differential tracking (left column) drifts after a few seconds. Tracking with only the first and the previous frame is inaccurate for long excursions away from the first frame, but tracking does not drift (center column). Adaptively adding new key frames provides the best accuracy and suffers no drift.

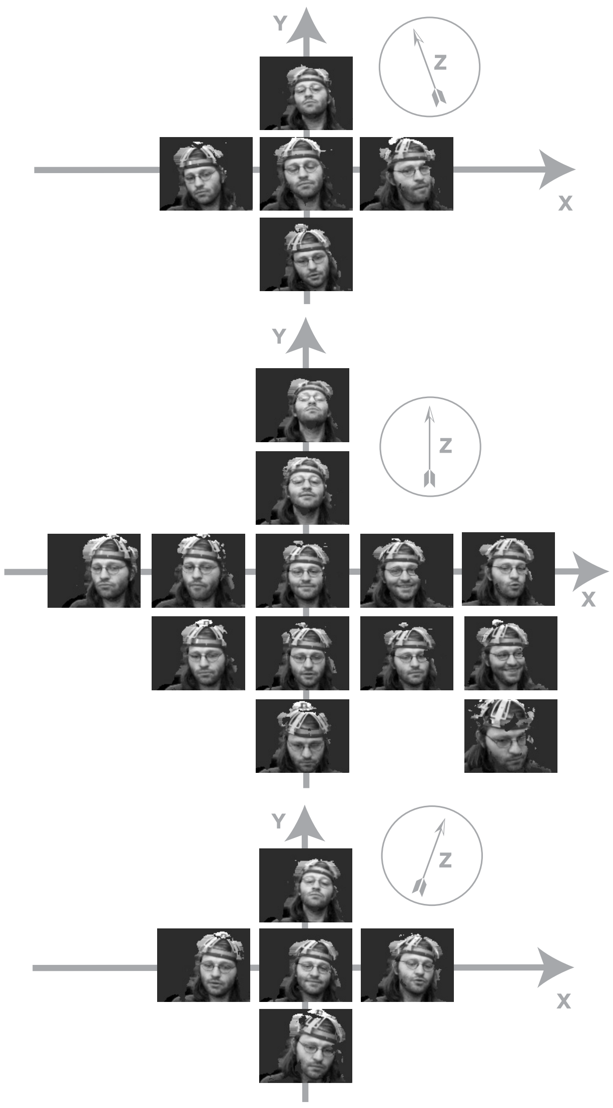

Fig. 7. The key frames acquired during one sequence, organized according to their pose. The key frames are spread evenly in the space of rotations to provide additional base frames for as many frames as possible.

for both large and small movements. Usually, the view-based tracker used 2 or 3 base frames (including the previous frame) to estimate each pose.

Figure 7 shows the key frames acquired during a tracking session. Figure 8 demonstrates how loop closures reduce drift and cause key frames to undergo adjustments.

To quantitatively analyze our algorithm, we compared our results to an *Inertia Cube*^{2} sensor from InterSense. *Inertia Cube*^{2} is an inertial 3-DOF orientation tracking system. The sensor was mounted on the inside structure of a construction hat. By sensing gravity and the earth's magnetic field, *Inertia Cube*^{2} estimates for the X and Z axes (where Z points outside the camera and Y

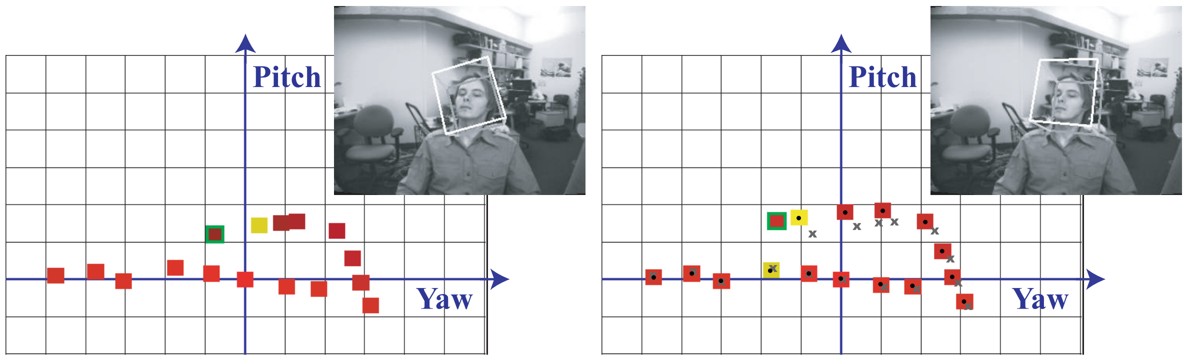

Fig. 8. Because key frames are correlated, closures can refine the pose of many key frames. The left panel shows two degrees of rotation of 15 key frames (solid squares) and of the current estimate of the pose of the head (outlined square). The light square is the key frame used for registration. It can be seen from the misalignment of the overlaid cube that the estimate pose of the head is slightly wrong. When the next frame becomes available, the current frame is compared against two key frames. Because one of these key frames was acquired much earlier, this closes a loop (right panel). The estimate of the pose of the head is corrected, and the key frames on the upper leg are adjusted as a result of the closure (the crosses depict the position of these key frames in the left panel).

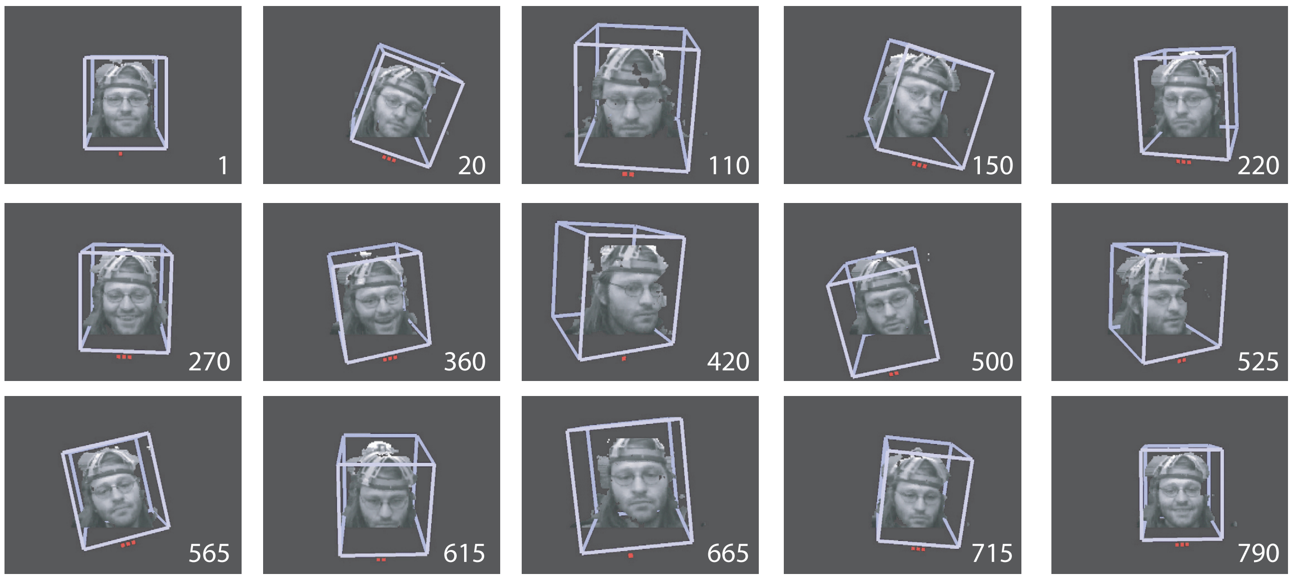

Fig. 9. To gather ground truth, the subject wore on his head an inertial sensor, whose output is compared with that of our adaptive view-based tracker in Figure 10.

points up) are mostly drift-free, but the Y-axis estimate can suffer from drift. InterSense reports an absolute pose accuracy of 3° RMS when the sensor is moving.

We recorded 4 sequences, using the *Inertia Cube*^{2} sensor. The sequences were

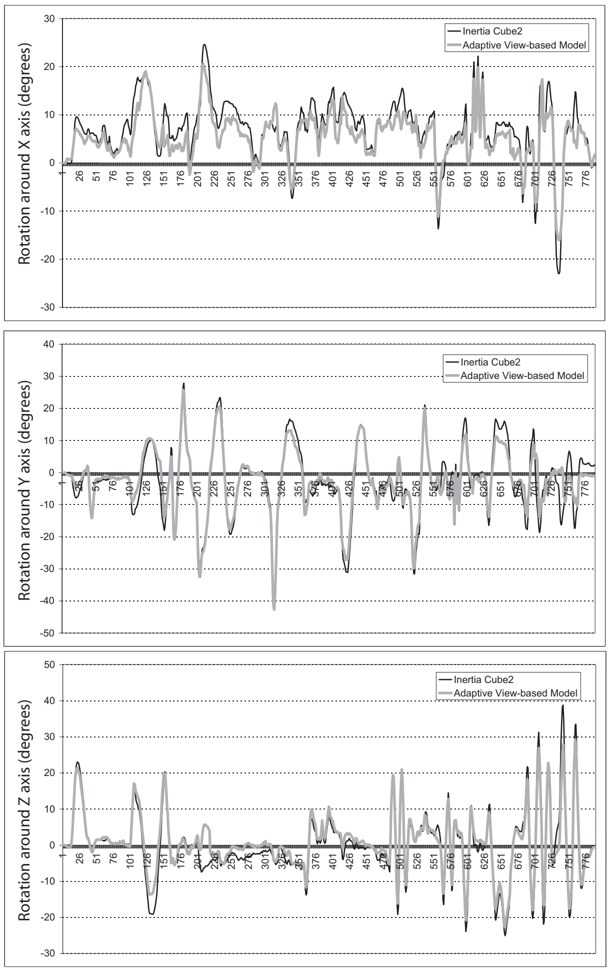

Fig. 10. Comparison of the head-pose estimation from our adaptive view-based approach with the measurements from the *Inertia Cube*^{2} sensor. The *Inertia Cube*^{2} only recovers rotations, so only the rotation axes are shown. The root mean squared difference between the output of the inertial sensor and our adaptive view-based tracker was about 2.8°, which is within the accuracy of the *Inertia Cube*^{2} itself.

recorded at 6 Hz and their average length was 801 frames (∼133 sec). During recording, subjects underwent rotations of about 125 degrees and translations of about 90 cm, including translation along the Z axis. Figure 9 shows the pose estimates of our adaptive view-based tracker for one of the sequences. Figure 10 compares the tracking results of this sequence with those of the inertial sensor. Since the inertial sensor can only recover rotations, we only compare these parameters. The average root mean squared distance to the output of the inertial sensor is 2.8°, which means our results are accurate to within the resolution of the *Inertia Cube*^{2} sensor.

8 Conclusion

We have shown how to turn pose-change estimators into accurate drift-free trackers. Our algorithms use pose-change estimators to track poses while simultaneously updating a view-based appearance model. This makes it relatively easy to build trackers, since pose change estimators are available off-the-shelf. We derived a Gaussian approximation to represent the uncertainty in the output of parametric pose-change estimators. Three tracking recipes were presented, each suitable for different situations. The batch method is exact and uses all frames as key frames. The online method of Section 5 is appropriate for situations where many key frames are needed, but it grows linearly in the number of frames used. By contrast, the complexity of the online method of Section 6 does not grow over time. This algorithm is well suited for situations where the appearance of the scene can be captured with a small number of key frames. Our experiments showed that these trackers can run for a very long time without significant drift.

A Uncertainty in Parametric Pose-Change Estimation

Some pose change estimators do not provide an uncertainty measure over their output. We present here a generic form for a distribution $p(y_{s,t}|x_s, x_t)$ that captures the uncertainty in the pose change estimate obtained from a large class of pose change estimators. We assume that $p(y_{s,t}|x_s, x_t)$ can be approximated by a Gaussian $\mathcal{N}(y_{s,t}|y^*, \Lambda_{s,t})$, where $y^* = x_t \ominus x_s$ is the true pose change, and proceed to derive a form for $\mathbf{\Lambda}_{s,t}$. We assume that the pose change estimator minimizes a least-squares registration error using a known motion model[2].

Note that $p(y_{s,t}|x_s, x_t)$ is a function of the true poses, but that registration algorithms operate on images. When the appearance of an image is largely governed by the pose, so that the distributions $p(I|x)$ are peaked, we have $p(y_{s,t}|x_s, x_t) \approx p(y_{s,t}|I_s, I_t)$ as a function of $y_{s,t}$. We therefore proceed by finding a Gaussian approximation to the distribution $p(y_{s,t}|I_s, I_t)$.

We assume that the pose change estimators in question are parametric motion estimators that search for the mode of the following distribution as a function

[2] An alternative idea, suggested by one of the anonymous reviewers, is that $p(y_{s,t}|x_s, x_t)$ can be learned from labeled data.

of $y_{s,t}$:

$$p(y_{s,t}|I_s, I_t) \propto \exp\left(-\frac{1}{2\sigma^2}\sum_{i\in\mathcal{P}}\left[I_s(i+u(i,y_{s,t})) - I_t(i)\right]^2\right), \tag{A.1}$$

where $\mathcal{P}$ are the pixels of I_t and the summation is over these pixels, and σ^2 is an unknown variance parameter. The function u warps a pixel i by an amount dictated by its second argument. Finding the mode of this distribution amounts to finding the pose change that minimizes the residual between the two images under the family of warpings u.

To approximate $p(y_{s,t}|I_s, I_t)$, we substitute the maximum likelihood estimate of σ, and set the mean y^* of the approximating Gaussian to $x_t \ominus x_s$, which will be near a mode of $p(y_{s,t}|I_s, I_t)$ when there is not much imaging noise. The covariance $\mathbf{\Lambda}_{s,t}$ will be set to the inverse curvature of $\log p(y_{s,t}|I_s, I_t)$ at $y_{s,t} = y^*$ following Laplace's approximation [8].

To justify this choice of covariance matrix, take the second order Taylor series expansion of $\log p(y_{s,t}|I_s, I_t)$ about y^*. The first order term vanishes because the first derivative is zero near the mode:

$$\log p(y_{s,t}|I_s, I_t) \approx \log p(y^*|I_s, I_t) + (y_{s,t} - y^*)^\top \mathbf{H}(y_{s,t} - y^*). \tag{A.2}$$

Exponentiating gives a Gaussian approximation to the posterior:

$$p(y_{s,t}|I_s, I_t) \approx \kappa \exp\left((y_{s,t} - y^*)^\top \mathbf{H}(y_{s,t} - y^*)\right) = \mathcal{N}\left(y_{s,t}\middle| y^*, -\frac{1}{2}\mathbf{H}^{-1}\right) \tag{A.3}$$

This approximation effectively fits a Gaussian near the mode of $p(y_{s,t}|I_s, I_t)$, matching its curvature there.

The Hessian of the log of the distribution in Equation (A.1) at $y_{s,t} = y^*$ is

$$\begin{aligned}\mathbf{H} = -\frac{1}{\hat{\sigma}^2}\sum_{i\in\mathcal{P}} &\dot{u}(i,y^*)^\top \nabla I_s(i+u(i,y^*))^\top \nabla I_s(i+p(i,y^*))\dot{u}(i,y^*) \\ &+ r(y^*)\nabla^2 I_s(i+u(i,y^*)),\end{aligned} \tag{A.4}$$

where $r(y^*)$ is the residual of the images after warping I_s by y^*. At y^*, the residual is very small, and $I_s(i + u(i, y^*)) \approx I_t(i)$, so the Hessian at y^* can be approximated by

$$\mathbf{H} \approx -\frac{1}{\hat{\sigma}^2}\sum_{i\in\mathcal{P}} \dot{u}(i,y^*)^\top \nabla I_t(i)^\top \nabla I_t(i)\dot{u}(i,y^*) \tag{A.5}$$

Finally, the maximum likelihood estimate of σ can be found by differentiating

$p(y_{s,t}|I_s, I_t)$ with respect to σ, and setting to zero:

$$\hat{\sigma}^2 = \frac{1}{|\mathcal{P}|} \sum_{i \in P} \left[I_s(i + u(i, y^*)) - I_t(i) \right]^2 , \tag{A.6}$$

where $|\mathcal{P}|$ denotes the number of pixels in $\mathcal{P}$. Putting everything together, we get the Gaussian approximation

$$\begin{aligned} p(y_{s,t}|x_s, x_t) &\approx \mathcal{N}(y_{s,t}|y^*, \Lambda_{s,t}) & \text{(A.7)} \\ y^* &= x_t \ominus x_s & \text{(A.8)} \\ \mathbf{\Lambda}_{s,t} &= \hat{\sigma}^2 \left[\sum_{i \in \mathcal{P}} \dot{u}(i, y^*)^\top \nabla I_t(i)^\top \nabla I_t(i) \dot{u}(i, y^*) \right]^{-1} . & \text{(A.9)} \end{aligned}$$

Equation (A.9) has an intuitive interpretation. The variance $\hat{\sigma}^2$ is the RMS reconstruction error after warping according to the recovered pose change. The summation measures the average sensitivity of each component of u, weighted by the strength of the features in the image. This is because $\nabla I_t(i)^\top \nabla I_t(i)$ represents the strength of a feature at location x (see [35]), and $\dot{u}(i)$ is the sensitivity to $y_{s,t}$ at various points in the image.

In the translational case, $u(i, y) = i + y$. So $\frac{\partial}{\partial y} u(i, y) = \mathbf{I}$. The covariance becomes

$$\mathbf{\Lambda}_{translation} = \hat{\sigma}^2 \left[\sum_{i \in \mathcal{P}} \nabla I_t(i)^\top \nabla I_t(i) \right]^{-1} , \tag{A.10}$$

which is just the reconstruction error weighted by a measure of how textured the image is.

In the case of an affine tracker, the partial of u is:

$$\frac{\partial}{\partial y} u(i, y) = \begin{bmatrix} i_1 & i_2 & 1 & 0 & 0 & 0 \\ 0 & 0 & 0 & i_1 & i_2 & 1 \end{bmatrix} . \tag{A.11}$$

If we set $\nabla I_t(i)^\top \nabla I_t(i) = \mathbf{I}$, effectively assigning the same texture to all points, the covariance becomes

$$\mathbf{\Lambda}_{aff} = \hat{\sigma}^2 \left[\sum_{i \in \mathcal{P}} \begin{bmatrix} i_1^2 & i_1 i_2 & i_1 & & & \\ i_1 i_2 & i_2^2 & i_2 & & \mathbf{0} & \\ i_1 & i_2 & 1 & & & \\ & & & i_1^2 & i_1 i_2 & i_1 \\ & \mathbf{0} & & i_1 i_2 & i_2^2 & i_2 \\ & & & i_1 & i_2 & 1 \end{bmatrix} \right]^{-1} . \tag{A.12}$$

Consistent with intuition, points away from the center of the coordinate system reduce the uncertainty in the multiplicative portion of the affine transformation more than the central points. In addition all points contribute equally to the translation parameters.

B Minimum KL-Divergence Simplification of a Factored Distribution

We would like to approximate a distribution $p(X) = \prod_t p_t(x_t|\mathrm{Pa}[x_t])$ with a distribution $q(X) = \prod_t q_t(x_t|\mathrm{Qa}[x_t])$ whose factors $q_t(x_t|\mathrm{Qa}[x_t])$ depend on a subset of the variables that appear in the corresponding factors of p (ie, $\mathrm{Qa}[x_t] \subset \mathrm{Pa}[x_t]$). We want q to be as close as possible to p in the KL-divergence sense, where the KL-divergence between two distributions p and q is defined as $\mathrm{KL}\,(p\|q) = \int_X p(X) \ln \frac{p(X)}{q(X)}$. It is well known that the closest such q is obtained by dropping the additional edges from the factors of p.

To see this, expand the KL divergence:

$$\mathrm{KL}\,(p\|q) = \int_X p(X) \ln \frac{\prod_t p_t(x_t|\mathrm{Pa}[x_t])}{\prod_t q_t(x_t|\mathrm{Qa}[x_t])} \tag{B.1}$$

$$= \int_X p(X) \sum_t \ln \frac{p_t(x_t|\mathrm{Pa}[x_t])}{q_t(x_t|\mathrm{Qa}[x_t])} \tag{B.2}$$

$$= \sum_t \int_{x_t, \mathrm{Pa}[x_t]} p(x_t, \mathrm{Pa}[x_t]) \ln \frac{p_t(x_t|\mathrm{Pa}[x_t])}{q_t(x_t|\mathrm{Qa}[x_t])}. \tag{B.3}$$

Since each term in the summation can be optimized over q_t separately, after dropping terms that do not depend on q and flipping signs, we get

$$q_t^*(x_t|\mathrm{Qa}[x_t]) = \arg\max_{q_t} \int_{x_t, \mathrm{Pa}[x_t]} p_t(x_t, \mathrm{Pa}[x_t]) \ln q_t(x_t|\mathrm{Qa}[x_t]) \tag{B.4}$$

$$= \arg\max_{q_t} \int_{\mathrm{Qa}[x_t]} p(\mathrm{Qa}[x_t]) \int_{x_t} p_t(x_t|\mathrm{Qa}[x_t]) \ln q_t(x_t|\mathrm{Qa}[x_t]) \tag{B.5}$$

$$= p_t(x_t|\mathrm{Qa}[x_t]). \tag{B.6}$$

The last statement follows because the inner integral in Equation (B.5) is the KL divergence between $p_t(x_t|\mathrm{Qa}[x_t])$ and $q_t(x_t|\mathrm{Qa}[x_t])$.

References

[1] N. Ayache and O. Faugeras. Maintaining representations of the environment of a mobile robot. *IEEE Tran. Robot. Automat.*, 5(6):804–819, 1989.

[2] J.R. Bergen, P. Anandan, K.J. Hanna, and R. Hingorani. Hierarchical model-based motion estimation. In *European Conference on Computer Vision (ECCV)*, pages 237–252, 1992.

[3] P. J. Besl and N. D. McKay. A method for registration of 3-D shapes. *Pattern Analysis and Machine Intelligence (PAMI)*, 14(2):239–256, February 1992.

[4] Y. Chen and G. Medioni. Object modelling by registration of multiple range images. In *International Conference on Robotics and Automation*, pages 2724–2728, 1991.

[5] A. Chiuso, P. Favaro, H. Jin, and S. Soatto. Structure from motion causally integrated over time. *Pattern Analysis and Machine Intelligence (PAMI)*, 24(4):523–535, April 2002.

[6] B. Curless. From range scans to 3D models. *Computer Graphics*, 33(4):38–41, November 1999.

[7] D. DeCarlo and D. Metaxas. Adjusting shape parameters using model-based optical flow residuals. *Pattern Analysis and Machine Intelligence (PAMI)*, 24(6):814–823, June 2002.

[8] A. Gelman, J. Carlin, H. Stern, and D. Rubinx. *Bayesian Data Analysis.* Chapman & Hall/CRC, 1995.

[9] J. Gutmann and K. Konolige. Incremental mapping of large cyclic environments. In *IEEE International Symposium on Computational Intelligence in Robotics and Automation (CIRA)*, 2000.

[10] M. Harville, A. Rahimi, T. Darrell, G.G. Gordon, and J. Woodfill. 3D pose tracking with linear depth and brightness constraints. In *International Conference on Computer Vision (ICCV)*, pages 206–213, 1999.

[11] B.K.P. Horn and E.J. Weldon, Jr. Direct methods for recovering motion. *International Journal of Computer Vision (IJCV)*, 2(1):51–76, June 1988.

[12] P.J. Huber. *Robust statistics.* Addison-Wesley, New York, 1981.

[13] T. Jebara and A. Pentland. Parametrized structure from motion for 3D adaptive feedback tracking of faces. In *Computer Vision and Pattern Recognition (CVPR)*, pages 144–152, 1997.

[14] A.D. Jepson, D.J. Fleet, and T. El-Maraghi. Robust on-line appearance models for visual tracking. In *Computer Vision and Pattern Recognition (CVPR)*, pages 415–422, 2001.

[15] H. Jin, P. Favaro, and S. Soatto. A semi-direct approach to structure from motion. *The Visual Computer*, 19:1–18, 2003.

[16] A. Kavčić and J.M.F. Moura. Matrices with banded inverses: inversion algorithms and factorization of gauss-markov processes. *IEEE Transactions on Information Theory*, 46(4):1495–1509, July 2000.

[17] T. Darrell L.-P. Morency, A. Rahimi. Fast 3d model acquisition from stereo images. In *3D Data Processing, Visualization and Transmission (3DPVT)*, 2002.

[18] M. LaCascia, S. Sclaroff, and V. Athitsos. Fast, reliable head tracking under varying illumination: An approach based on registration of textured-mapped 3D models. *Pattern Analysis and Machine Intelligence (PAMI)*, 22(4):322–336, April 2000.

[19] J. J. Leonard and P. M. Newman. Consistent, convergent, and constant-time SLAM. In *International Joint Conferences on Artificial Intelligence (IJCAI)*, pages 1143–1150, 2003.

[20] H. Lev-Ari, S.R. Parker, and T. Kailath. Multidimensional maximum-entropy covariance extension. *IEEE Transactions on Information Theory*, 35:497–508, May 1989.

[21] F. Lu and E. Milios. Globally consistent range scan alignment for environment mapping. *Autonomous Robots*, 4:333–349, 1997.

[22] F. Lu and E. Milios. Robot pose estimation in unknown environments by matching 2D range scans. *Robotics and Autonomous Systems*, 22(2):159–178, 1997.

[23] B. D. Lucas and T. Kanade. An iterative image registration technique with an application to stereo vision. In *International Joint Conference on Artificial Intelligence*, pages 674–679, 1981.

[24] P. F. McLauchlan. A batch/recursive algorithm for 3D scene reconstruction. *Computer Vision and Pattern Recognition (CVPR)*, 2:738–743, 2000.

[25] T.P. Minka. Expectation propagation for approximate bayesian inference. In *Uncertainty in Artificial Intelligence (UAI)*, pages 362–369, 2001.

[26] T.P. Minka. Old and new matrix algebra useful for statistics. Technical report, Media Lab, `http://www.media.mit.edu/~tpminka/papers/matrix.html`, 2001.

[27] L.-P. Morency and T. Darrell. Stereo tracking using ICP and normal flow constraint. In *International Conference on Pattern Recognition (ICPR)*, pages 367–372, 2002.

[28] L-P. Morency, A. Rahimi, and T. Darrell. Adaptive view-based appearance models. In *Computer Vision and Pattern Recognition (CVPR)*, pages 803–812, 2003.

[29] R. M. Murray, Z. Li, and S. S. Sastry. *A Mathematical Introduction to Robotic Manipulation.* CRC Press, 1994.

[30] A. Papoulis. *Probability, random variables, and stochastic processes.* McGraw-Hill, New York, third edition, 1991.

[31] K. Pulli. Multiview registration for large data sets. In *Int.Conf. on 3D Digital Imaging and Modeling*, pages 160–168, 1999.

[32] A. Rahimi and T. Darrell. Location estimation with a differential update network. In *Neural Information Processing Systems (NIPS)*, pages 1049–1056, 2002.

[33] A. Rahimi, L-P. Morency, and T. Darrell. Reducing drift in parametric motion tracking. In *International Conference on Computer Vision (ICCV)*, volume 1, pages 315–322, June 2001.

[34] H. S. Sawhney, S. Hsu, and R. Kumar. Robust video mosaicing through topology inference and local to global alignment. In *European Conference on Computer Vision (ECCV)*, pages 103–119, 1998.

[35] J. Shi and C. Tomasi. Good features to track. In *Computer Vision and Pattern Recognition (CVPR)*, pages 593–600, 1994.

[36] H.-Y. Shum and R. Szeliski. Construction of panoramic mosaics with global and local alignment. In *International Journal of Computer Vision (IJCV)*, pages 101–130, February 2000.

[37] A. Stoddart and A. Hilton. Registration of multiple point sets. In *International Conference on Pattern Recognition (ICPR)*, volume 2, pages 40–44, 1996.

[38] S. Thrun. A probabilistic online mapping algorithm for teams of mobile robots. *International Journal of Robotics Research*, 20(5):335–363, 2001.

[39] G. Turk and M. Levoy. Zippered polygon meshes form range images. In *SIGGRAPH*, pages 311–318, 1994.

[40] L. Vacchetti, V. Lepetit, and P. Fua. Fusing online and offline information for stable 3-D tracking in real-time. In *Computer Vision and Pattern Recognition (CVPR)*, pages 241–249, 2003.

[41] Videre Design. *MEGA-D megapixel digital stereo head.* `http://www.ai.sri.com/~konolige/svs`, 2000.

[42] P. Viola and M. Jones. Robust real-time face detection. *International Journal of Computer Vision (IJCV)*, 57:137–154, May 2004.